ACS APPLIED MATERIALS & INTERFACES

Research Article

www.acsami.org

Additive-Assisted Control over Phase-Separated Nanostructures by Manipulating Alkylthienyl Position at Donor Backbone for Solution-Processed, Non-Fullerene, All-Small-Molecule Solar Cells

Jianhua Huang,[†] Xue Wang,[†,‡] Xin Zhang,[†] Zhixiao Niu,[†,‡] Zhenhuan Lu,[†] Bo Jiang,[†] Yuxi Sun,[‡] Chuanlang Zhan,*[,†] and Jiannian Yao*[,†]

[†]Beijing National Laboratory for Molecular Sciences, CAS Key Laboratory of Photochemistry, Institute of Chemistry, Chinese Academy of Sciences, Beijing 100190, P. R. China.

[‡]Key Laboratory of Life-Organic Analysis, QuFu Normal University, QuFu 273165, P. R. China.

Supporting Information

ABSTRACT: A non-fullerene, all-small-molecule solar cell (NF-SMSC) device uses the blend of a small molecule donor and a small molecule acceptor as the active layer. Aggregation ability is a key factor for this type of solar cell. Herein, we used the alkylthienyl unit to tune the aggregation ability of the diketopyrrolopyrrole (DPP)-based small molecule donors. Replacing two alkoxyl units in **BDT-O-DPP** with two alkylthienyl units yields **BDT-T-DPP**, and further introducing another two alkylthienyl units into the backbone produces **BDT-T-2T-DPP**. With the introduction of alkylthienyl, the backbone becomes twisted. As a result, the $\pi\pi$-stacking strength, aggregation ability, and crystallite size all obey the sequence of **BDT-O-DPP** > **BDT-T-DPP** > **BDT-T-2T-DPP**. When selected a reported perylene diimide dimer of bis-PDI-T-EG as acceptor, the best NF-SMSC device exhibits a power conversion efficiency of 1.34, 2.01, and 1.62%, respectively, for the **BDT-O-DPP**, **BDT-T-DPP**, and **BDT-T-2T-DPP** based system. The **BDT-T-DPP**/bis-PDI-T-EG system yields the best efficiency of 2.01% among the three combinations. This is due to the moderate aggregation ability of **BDT-T-DPP** yields moderate phase size of 30−50 nm, whereas the strong aggregation ability of **BDT-O-DPP** gives a bigger size of 50−80 nm, and the weak aggregation ability of **BDT-T-2T-DPP** produces a smaller size of 10−30 nm. The **BDT-T-DPP**/bis-PDI-T-EG combination exhibits balanced hole/electron mobility of 0.022/0.016 $cm^2/(V\ s)$, whereas the **BDT-O-DPP**/bis-PDI-T-EG and the **BDT-T-2T-DPP**/bis-PDI-T-EG blend show a hole/electron mobility of 0.0011/0.0057 $cm^2/(V\ s)$ and 0.0016/0.11 $cm^2/(V\ s)$, respectively.

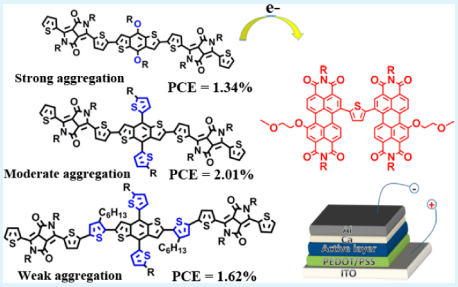

KEYWORDS: *solution-processed, non-fullerene, all-small-molecule solar cell, phase-separated nanostructure, alkylthienyl position, donor backbone*

1. INTRODUCTION

The past decades have witnessed a great success in polymer solar cells (PSCs, Figure 1),[1−4] in which a conjugated polymer as donor material and a fullerene derivative, e.g. [6,6]-phenyl-C_{61} (or C_{71})-butyric acid methyl ester (PC61BM or PC71BM), as acceptor material were blended to be a nano-phase separated bulk heterojunction (BHJ), acting as a photo-sensitive layer. The polymer materials usually suffer several drawbacks, such as a broad molecular weight distribution and batch-to-batch variations.[5,6] To this end, small molecule donors, being regarded as proper alternatives to polymer donors, have been intensively researched recently.[7] Several kinds of small molecules were synthesized as donor materials to match with PCBM, for example, in energy levels, to prepare small molecule solar cells (SM-SCs, Figure 1).[8−28] Among those donor materials, some promising structures exhibit excellent photovoltaic performances with power conversion efficiency (PCE) exceeding 8% when they were combined with the widely-used PCBM acceptor material through judicious device optimizations and architecture innovations.[6,29] In another aspect, fullerene derivatives, currently playing a dominant role as acceptor material, also bear several drawbacks: (1) There are no hydrogen atoms covalently linked to the fullerene backbone and adduction reaction is the most frequently used way to chemically modify the fullerene backbone. Following these reactions, the energy level of the lowest unoccupied molecular orbitals (LUMOs) is raised by breaking down the conjugation of the π-electrons.[30] While it is difficult to establish the conjugation between the π-electrons of the fullerene and those of the covalently attached functions, which limits the fine-tuning on its optoelectronic properties, for example, shifting the absorption to the long wavelength range and further enhancing the absorptivity in the visible and near infrared (IR) region, and (2) the adduction reaction on the fullerene backbone is weakly selective and this not only lowers the yield of the target product but also magnifies the purification difficulty. Given that the

Received: October 18, 2013
Accepted: February 21, 2014
Published: February 21, 2014

   dx.doi.org/10.1021/am406050j | ACS Appl. Mater. Interfaces 2014, 6, 3853−3862

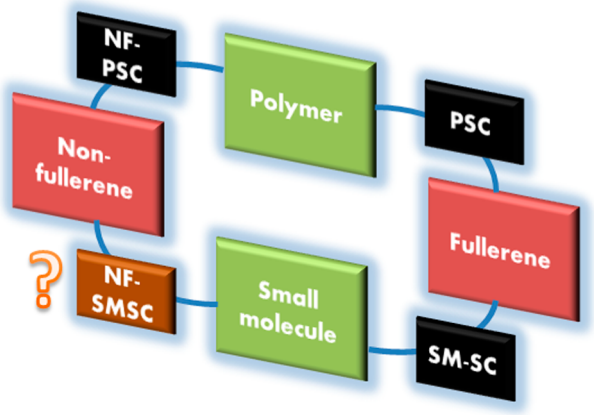

Figure 1. Classes of organic solar cells classified by the donor/acceptor materials.

impurity may severely detriment the power conversion efficiency of PCBM, it needs special equipment like high performance liquid chromatography (HPLC) to produce high-quality PCBM,[31] which then elevates the PCBM's price and limits the practical applications. Therefore, non-fullerene acceptor materials with strong light-harvesting ability, suitable energy levels, and proper crystallization have been also paid much attention in the past decades.[32,33] Several n-type organic semiconductors, including n-type polymers[34−36] and small molecules[37−47] have been developed to match with p-type polymer donors such as P3HT,[34,38−40,45,46,48] PT1,[35] and PBDTTT-C-T[49] to fabricate non-fullerene solar cells (NF-PSCs, Figure 1), exhibiting an efficiency, exceeding 2%. Recently, we reported an n-type perylene diimide (PDI) dimer-based (so called bis-PDI-T-EG, Scheme 1) acceptor material, exhibiting a record efficiency of 4.03% when matching with PBDTTT-C-T.[50]

Scheme 1. Molecular Structures of Three DPP-Based Donor Molecules, BDT-O-DPP, BDT-T-DPP, and BDT-T-2T-DPP and the PDI-Based Acceptor Molecule of Bis-PDI-T-EG

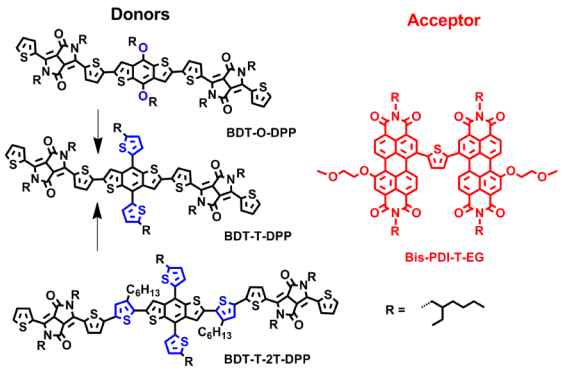

Although a lot of studies have been focused on looking for alternatives to one component in the heterojunction active layers of PSCs, e.g., replacing polymer donors with small molecule donors, keeping the fullerene derivatives as acceptor material (SM-SCs) or replacing fullerene acceptors with non-fullerene polymer or small molecule acceptors, keeping the polymers as donor materials (NF-PSCs), as mentioned above, those studies will not simultaneously avoid the drawbacks of polymers and fullerene derivatives in a BHJ solar cell. In order to realize a satisfying compromise, herein, we try to prepare another kind of OSC, with an organic small molecule used as donor material and a non-fullerene small molecule used as acceptor material, which can be named as non-fullerene, all-small-molecule solar cells (NF-SMSCs), as shown in Figure 1. That device can be a thorough alternative to the classic PSCs and will avoid the drawbacks of both polymers and fullerene-derivatives. However, NF-SMSCs are still scarcely studied probably because of the over-aggregation of small molecules and the poor film morphology of the BHJ films.[51,52]

It's known to all that the molecular packing ordering and nano-phase size are two essential factors that affect the photovoltaic performance of organic photosensitive layer. For example, the $\pi\pi$-stacking order can strongly affects the exciton and charge transport[53] and the nano-phase size determines the exciton diffusion/separation efficiency and usually several tens nanometer domains will be favorable for these processes.[54] To understand the structure−property relationships, herein we designed three DPP-based small molecules, **BDT-O-DPP**, **BDT-T-DPP**, and **BDT-T-2T-DPP**, respectively, as donor material (Scheme 1). The PDI dimer of bis-PDI-T-EG was selected as the non-fullerene acceptor material to prepare NF-SMSCs. The phase separated nanostructures of the NF-SMSCs were adjusted by anchoring the alkylthienyl at different positions of the donor backbone. For **BDT-O-DPP**, the molecular aggregation is strong because of the strong dipolar interaction of oxygen atom and the size of nanophase separation is 50−80 nm, leading to a PCE of 1.34%. For **BDT-T-DPP**, in which the alkoxyl group is replaced by alkylthienyl, the aggregation is decreased and the size of nano-phase separation is 30−50 nm, leading to a PCE of 2.01%. For **BDT-T-2T-DPP**, in which two alkylthienyl groups are further introduced in the backbone, the aggregation is further weakened and the size of nano-phase separation is 10−30 nm, leading to a PCE of 1.62%. **BDT-T-DPP** exhibits the highest PCE of 2.01% among the three molecules because of its proper aggregation ability and favorable nanosized phase separation.

2. RESULTS AND DISCUSSION

The synthetic routes towards the three DPP-based donor molecules are shown in Scheme 2. For **BDT-O-DPP** and **BDT-T-DPP**, the Stille coupling reaction between commercially

Scheme 2. Synthetic Routes to BDT-O-DPP, BDT-T-DPP, and BDT-T-2T-DPP[a]

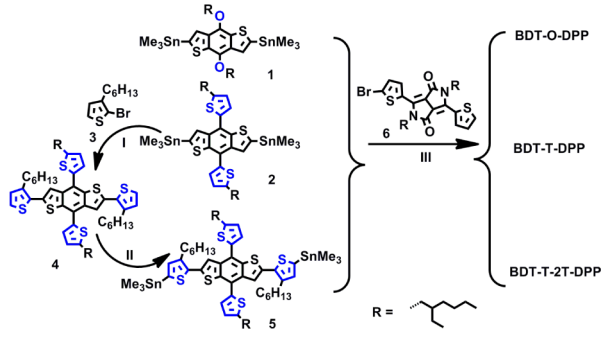

[a]Reaction conditions: (I) $Pd(PPh_3)_4$, toluene, reflux, overnight; (II) n-BuLi, THF, −30 °C, then Me_3SnCl; (III) $Pd_2(dba)_3$, $P(toyl)_3$, toluene, reflux, overnight. All the reactions were protected under N_2 atmosphere.

dx.doi.org/10.1021/am406050j | ACS Appl. Mater. Interfaces 2014, 6, 3853−3862

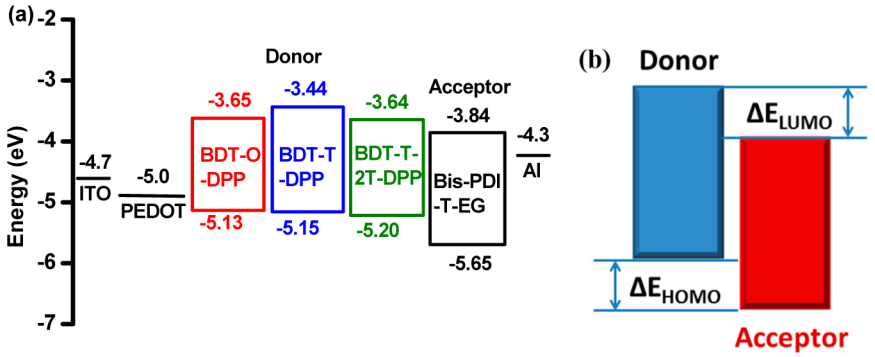

Figure 2. (a) Energy level diagram of the DPP-based molecules, bis-PDI-T-EG, and other components in a conventional organic photovoltaic device and (b) schematic diagram of ΔE_{HOMO} and ΔE_{LUMO}.

available reactants **1** or **2** with the compound **6** afforded the final products with a high conversion yield of 80 and 82%, respectively.[55] For **BDT-T-2T-DPP**, the starting material **2** was firstly reacted with **3** to obtain **4** with a yield of 78%. Then, **4** was reacted with n-BuLi and Me_3SnCl, yielding the ditinated products **5**. Metastable **5** was used without further purification and reacted with **6** to obtain **BDT-T-2T-DPP**. The three DPP-based molecules exhibit good solubility in the commonly used solvents, such as dichloromethane, chloroform, chlorobenzene, and *o*-dichlorobenzene. All three molecules were fully characterized with ^{1}H NMR, ^{13}C NMR, TOF-MS, and element analysis, as shown in the Experimental Section.

The thermal stability of the three molecules was characterized by thermogravimetric analysis (TGA) and the data were summarized in Table S1 in the Supporting Information. As shown in Figure S1 in the Supporting Information, the decomposed temperature (T_m) at 5% weight loss for **BDT-O-DPP**, **BDT-T-DPP**, and **BDT-T-2T-DPP** is 358, 409, and 405 °C, respectively, which are all thermal stable enough for use in organic solar cells.

The electrochemical properties of the three DPP-based donors and the bis-PDI-T-EG acceptor were measured using cyclic voltammetry (CV) (see Figure S2 in the Supporting Information) and summarized in Table S1 in the Supporting Information. The highest occupied molecular orbitals (HOMO) energy of the three DPP-based molecules were estimated from the onset voltage of oxidation process ($E_{onset(ox)}$) in formula $E_{HOMO} = -(4.4 + E_{onset(ox)})$ eV,[56] as −5.13, −5.15, and −5.20 eV for **BDT-O-DPP**, **BDT-T-DPP**, and **BDT-T-2T-DPP**, respectively. The lowest unoccupied molecular orbitals (LUMO) energy calculated using $E_{LUMO} = -(4.4 + E_{onset(red)})$, where $E_{onset(red)}$ is the onset voltage of reduction process, is −3.65, −3.44, and −3.64 eV for **BDT-O-DPP**, **BDT-T-DPP**, and **BDT-T-2T-DPP**, respectively. Figure 2a shows the energy level diagram of the three DPP-based molecules, bis-PDI-T-EG, and other components in a photovoltaic device.

As the energy level match of donor and acceptor in a heterojunction solar cell device plays an essential role in the balanced charge dissociation, herein we use the LUMO energy offset (ΔE_{LUMO}) and HOMO energy offset (ΔE_{HOMO}) of donor/acceptor to evaluate the degree of energy level match between each of the three DPP-based molecules and bis-PDI-T-EG, as schematically shown in Figure 2b. The values of $\Delta E_{LUMO}/\Delta E_{HOMO}$ are 0.19 eV/0.52 eV, 0.40 eV/0.50 eV, and 0.20 eV/0.45 eV, respectively, for **BDT-O-DPP**, **BDT-T-DPP**, and **BDT-T-2T-DPP**. Among the three donor molecules, **BDT-T-DPP** exhibits the closest ΔE_{HOMO} and ΔE_{LUMO} values with bis-PDI-T-EG as acceptor, indicating the balanced HOMO−HOMO and LUMO−LUMO energy match with the acceptor among the three donor molecules.

Optimal conformations of the three donor molecules were obtained by molecular modelling on Gaussian 09 at the B3LYP/6-31G* level of theory in the gas phase. As shown in Figure 3a–d, backbone of **BDT-O-DPP** and **BDT-T-DPP** displays good planarity. The dihedral angles of θ (12-34) and θ

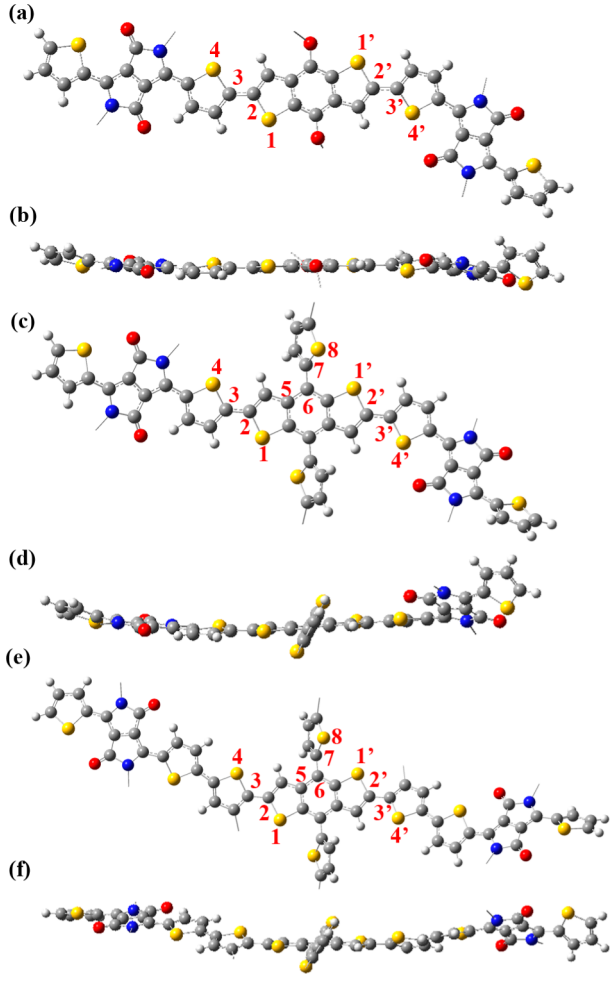

Figure 3. Optimal molecular conformations of (a, b) **BDT-O-DPP**, (c, d) **BDT-T-DPP**, and (e, f) **BDT-T-2T-DPP**. For clarity, the alkyl chains are not shown.

dx.doi.org/10.1021/am406050j | ACS Appl. Mater. Interfaces 2014, 6, 3853−3862

Table 1. Conformation and Absorption Parameters of Pristine BDT-O-DPP, BDT-T-DPP, BDT-T-2T-DPP, and the Respective Blend Films with Bis-PDI-T-EG

	θ^a (deg)			ε_{max} ($M^{-1}cm^{-1}$)^b	λ_{max} (nm)^c/fwhm (nm)^d		$A_0/A_1{}^e$	
compds	12-34	1′2-′3′4′	56-78	solution	solution	film	film	ΔH_m (J/g)^f
BDT-O-DPP	170	−166		1.26×10^5	620/120	618, 667/170	0.98	58.18
BDT-T-DPP	174	172	122	1.42×10^5	624/129	629, 679/177	0.91	45.44
BDT-T-2T-DPP	157	157	122	1.20×10^5	598/125	620, 671/164	0.88	39.47
BDT-O-DPP/bis-PDI-T-EG						606, 657/185	0.77	
BDT-T-DPP/bis-PDI-T-EG						612, 672/184	0.70	
BDT-T-2T-DPP/bis-PDI-T-EG						604, 657/200	0.69	

[a]Dihedral angle illustrated in Figure 3. [b]Molar extinction coefficient in chloroform. [c]Wavelength of absorption maximum. [d]Full width at half maximum (fwhm). [e]Absorbance ratio at 670 nm vs. 610 nm in film. [f]Melting enthalpy.

(1′2′-3′4′) are about 170° and −170°, respectively, for both molecules (Table 1). However, the pendant thiophene on the benzodithiphene of **BDT-T-DPP** is twisted with respect to the backbone in a dihedral angle of θ (56-78) = 122° (Figure 3c, d). Compared to the former two molecules, **BDT-T-2T-DPP**'s backbone exhibits poorer planarity with θ (12-34) = 157° and θ (1′2′-3′4′) = 157° (Figure 3e, f), due to introduction of another two thiophenes into the main chain. Accordingly, the backbone planarity of the three molecules obeys the following sequence: **BDT-O-DPP** > **BDT-T-DPP** > **BDT-T-2T-DPP**. Those results indicate that the molecular conformations of the three molecules are finely tuned by anchoring the alkylthienyl at different positions of the donor backbone.

Figure 4 shows the UV−vis absorption spectra of the three DPP-based molecules and bis-PDI-T-EG, all in chloroform.

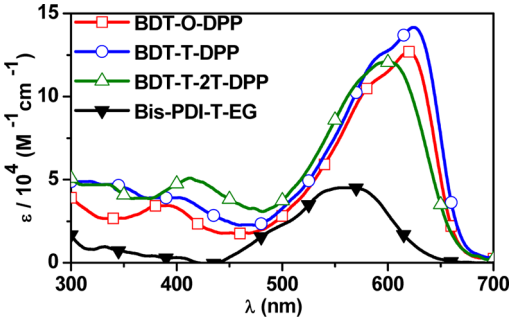

Figure 4. UV−vis absorption spectra of the three donors and bis-PDI-T-EG in chloroform solution, all at a dilute concentration of 1×10^{-6} M.

Table 1 summarizes the optical properties of the three molecules. All the three DPP-based molecules display an absorption peak at 590—630 nm, which is ascribed to the intramolecular charge transfer (ICT) absorption.[11] **BDT-O-DPP** shows an absorption peak ($\lambda^{sol}{}_{max}$) at 620 nm, with a full width at half maximum (fwhm) of 120 nm. After the alkoxyl group in **BDT-O-DPP** is replaced by the alkylthienyl pendant, the resulting molecule, **BDT-T-DPP**, displays a slightly red-shifted $\lambda^{sol}{}_{max}$ of 624 nm and a slightly increased value of fwhm, 129 nm, which attributes to the enlarged two-dimensional conjugation.[57] Further introducing another two alkylthienyl in the backbone between the DPP and BDT units decreases the planarity of the backbone. The resulting **BDT-T-2T-DPP** exhibits a blue-shifted $\lambda^{sol}{}_{max}$ of 598 nm and a slightly decreased fwhm value of 125 nm, compared to **BDT-T-DPP**. The maximum molar extinction coefficient (ε_{max}) of **BDT-T-DPP** (1.42×10^5 M^{-1} cm^{-1}) is larger than that of **BDT-O−DPP** (1.26×10^5 M^{-1} cm^{-1}) due to the enhanced conjugation, and also it is greater than that of **BDT-T-2T-DPP** (1.20×10^5 M^{-1} cm^{-1}) because of the decreased backbone planarity of **BDT-T-2T-DPP**. Bis-PDI-T-EG shows an absorption peak at 560 nm with an ε_{max} value of 5.6×10^4 M^{-1} cm^{-1} in solution and a strong and broad absorption from 300 to 650 nm.[50]

As the donor molecules form into aggregates in solid film, the film shows a significantly different film absorption spectrum in comparison to the solution absorption spectrum (see Figure S3 in the Supporting Information). In the pristine donor film, two absorption bands are observed. One appears around 610 nm, and the other occur around 670 nm. The former one is close to the ICT band, as observed in the solution spectrum, whereas the latter one, which is absent in the solution spectrum, appears after the donor molecules form aggregates in film. Appearance of the latter absorption band is due to (1) the planarization of the backbone and (2) formation of $\pi\pi$-stacks as molecules form into aggregates in the film. Similar phenomenon is observed from other small molecule donor molecules.[25,58] Considering the fact that the 670 nm absorption is not seen in the dilute solution, while it appears only in the solid film, the 610 and 670 nm absorption bands are not related

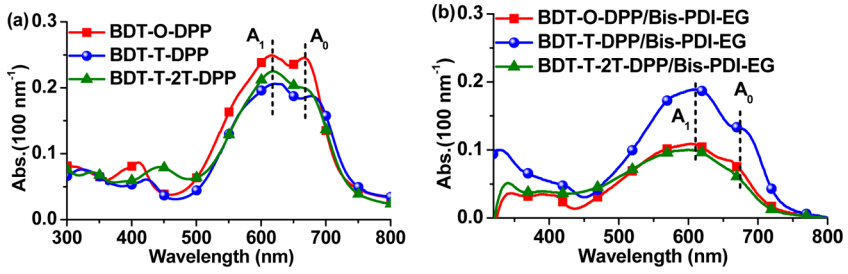

Figure 5. Film absorption spectra of (a) neat **BDT-O-DPP**, **BDT-T-DPP**, and **BDT-T-2T-DPP** films and (b) blend films with bis-PDI-T-EG. Films were all prepared from the corresponding chloroform solutions.

dx.doi.org/10.1021/am406050j | ACS Appl. Mater. Interfaces 2014, 6, 3853−3862

to a vibronic progression of the same electronic transition, while potentially correspond to two different electronic species — the 610 nm absorption band arises from the intramolecular exciton transition, whereas the 670 nm band is due to the formation of intermolecular aggregates. Conformation difference as indicated from the optimal conformation (Figure 3) affects the backbone planarity and $\pi\pi$-stacking strength in the solid aggregates. As a result, the relative absorbance of 670 nm (A_0) to 610 nm (A_1), A_0/A_1, varies through changing the alkylthienyl position at the backbone (Figure 5a). Table 1 summarizes the A_0/A_1 value of the neat donor and blend film.

The neat **BDT-O−DPP** film spun-cast from the chloroform solution shows an A_0/A_1 value of 0.98. After the alkoxyl group is replaced by the alkylthienyl, the resulted **BDT-T-DPP** film shows a decreased A_0/A_1 value of 0.91. Moreover, when another two alkylthienyl groups are further introduced into the backbone, the **BDT-T-2T-DPP** film gives a lowest A_0/A_1 value of 0.88. The A_0/A_1 value obeys the following sequence: **BDT-O-DPP** (0.98) > **BDT-T-DPP** (0.91) > **BDT-T-2T-DPP** (0.88), which is consistent well with that conformation-twist tendency, decreasing from **BDT-O-DPP** to **BDT-T-DPP** and then to **BDT-T-2T-DPP**. This tendency of $\pi\pi$-stacking strength agrees well with the (010) diffraction from the X-ray diffraction (XRD) data of the neat donor film (see Figure S4b in the Supporting Information). **BDT-O-DPP** shows an obvious peak at Q = 1.66 Å^{-1}, corresponding to a $\pi\pi$-distance of 3.77 Å. For **BDT-T-DPP**, a larger $\pi\pi$-distance of 3.90 Å (Q = 1.61 Å^{-1}) is observed. For **BDT-T-2T-DPP**, only a very weak, broad (010) diffraction band is observed around Q = 1.65 Å^{-1}. Similar phenomenon is observed in the blended films. As shown in Figure 5b, the blended film prepared from the cprresponding chloroform solution gives an A_0/A_1 value following the sequence of **BDT-O-DPP**/bis-PDI-T-EG (0.77) > **BDT-T-DPP**/bis-PDI-T-EG (0.70) > **BDT-T-2T-DPP**/bis-PDI-T-EG (0.69).

The conformation variation is expected to change the aggregation ability. As such, differential scanning calorimetry (DSC) was firstly tested to study the crystallization of the three donor molecules. The DSC curves of the three DPP-based molecules show well-defined melting and crystallization peaks (Figure 6). The melting enthalpy (ΔH_m) of the three

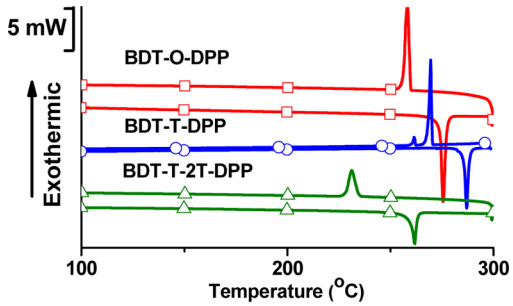

Figure 6. DSC curves of the DPP-based molecules.

molecules, calculated from the integrated area of melting peak obeys the sequence of **BDT-O−DPP** (58.18 J/g) > **BDT-T-DPP** (45.44 J/g) > **BDT-T-2T-DPP** (39.47 J/g), as shown in Table 1. **BDT-O-DPP** exhibits the highest ΔH_m value among the three molecules, indicating the highest crystallinity and strongest aggregation properties, which results from the strong dipolar interaction between the alkoxyl groups and good backbone planarity. After replacing the alkoxyl with the alkylthienyl, **BDT-T-DPP** shows lower crystallinity and aggregation due to the weaker dipolar interaction of alkylthienyl and the twist conformation between the thiophene unit and the backbone, as indicated in our previous work.[59] After another two alkylthienyl units are further introduced into the main chain in between the BDT and DPP units, the **BDT-T-2T-DPP** exhibits even lower ΔH_m, due to the poor backbone planarity, which weakens $\pi\pi$-stacking of the molecular main chains in the solid state. Those results indicate that the alkylthienyl can be a useful unit to adjust the crystallization ability of small-molecule-based donors.

XRD experiments was used to evaluate the crystallite sizes to get a deeper insight into the fine-tuning of crystallization ability by altering the alkylthienyl positions. The samples were prepared by drop-coating the corresponding chloroform solutions on silica substrates and thermal annealing at 100 °C for 30 min. Table 2 summarized the diffraction parameters for

Table 2. XRD Parameters of Neat BDT-O-DPP, BDT-T-DPP, and BDT-T-2T-DPP Films and Blend Films with Bis-PDI-T-EG[a]

compds	Q (Å^{-1})[b]/d (Å)[c]	L (nm)[d]
BDT-O-DPP	0.40/15.8	52.0
BDT-T-DPP	0.37/17.1	24.5
BDT-T-2T-DPP	0.36/17.8	8.2
BDT-O-DPP/bis-PDI-T-EG	0.40/15.8	35.0
BDT-T-DPP/bis-PDI-T-EG	0.35/17.9	8.6
BDT-T-2T-DPP/bis-PDI-T-EG	0.41/16.7	6.7

[a]Films were all prepared by drop-coating the corresponding chloroform solutions on silica substrates and thermal annealing at 100 °C. [b]The diffraction vector at (100) direction. [c]Spacing calculated by $d = 2\pi/Q$. [d]The crystallite size estimated by the Scherrer Equation.

the (100) stacking. As shown in Figure S4a in the Supporting Information, the pristine **BDT-O-DPP**, **BDT-T-DPP** and **BDT-T-2T-DPP** show a sharp and strong (100) diffraction peak at Q = 0.40 Å^{-1} (d = 15.8 Å), 0.37 Å^{-1} (d = 17.1 Å), and 0.36 Å^{-1} (d = 17.8 Å^{-1}), respectively. The crystallite sizes were estimated from the Scherrer equation,[60] $L = 4K\lambda/(\beta Q)$, where L is the crystallite size, K Scherrer constants, β the full width at half maximum of the diffraction peak in radians, λ the incident wavelength, Q the diffraction vector.

As summarized in Table 2, the pristine **BDT-O-DPP** film shows a large crystallite size of 52.0 nm. After the alkoxyl group is replaced by alkylthienyl, **BDT-T-DPP** displays a reduced crystallite size of 24.5 nm. Furthermore, when two alkylthienyl groups are introduced into the backbone, **BDT-T-2T-DPP** exhibits an even smaller crystallite size of 8.2 nm. This decreased crystallite size from **BDT-O-DPP** to **BDT-T-DPP**, and to **BDT-T-2T-DPP** is well-consistent with the crystallization ability, which is well-adjusted by anchoring the alkylthienyl onto the different positions of the backbone. This decreasing trend of the aggregation ability is maintained after the donor is blended with bis-PDI-T-EG, as shown in Table 2.

NF-SMSC devices were prepared with bis-PDI-T-EG as the non-fullerene acceptor and **BDT-O-DPP**, **BDT-T-DPP**, and **BDT-T-2T-DPP**, respectively, as the donor based on the conventional device configuration of ITO/PEDOT: PSS/active layer/Ca/Al. After processing optimizations by screening the D/A weight ratio and the 1,8-diiodooctane (DIO) content, best devices were obtained and their device parameters are summarized in Table S2 in the Supporting Information. We

dx.doi.org/10.1021/am406050j | ACS Appl. Mater. Interfaces 2014, 6, 3853−3862

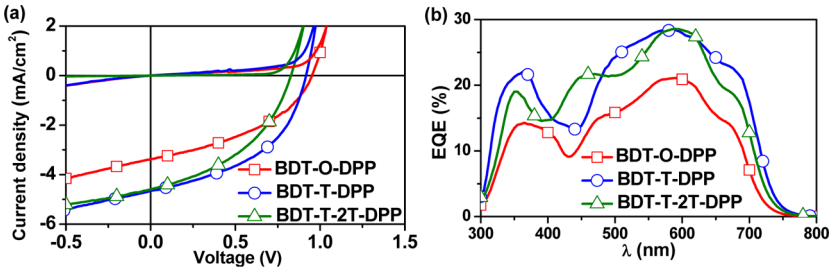

Figure 7. (a) $J-V$ curves and (b) EQE curves of the best NF-SMSC devices based on **BDT-O-DPP**, **BDT-T-DPP**, and **BDT-T-2T-DPP**, as the donor and bis-PDI-T-EG as the acceptor, respectively.

used DIO as the co-solvent to optimize film morphology in the active layer. The best device obtained through screening the DIO content implies that the molecular optoelectronic advantages of the donor have been translated into device properties to the highest degree via optimizing film morphology and this provides the basis for the further structure-property correlation between these three donors. Figure 7a shows the $J-V$ curves of the champion devices based on the three molecules. Table 3 shows the photovoltaic parameters of the champion NF-SMSC devices. For **BDT-O-DPP**-based NF-SMSCs, the champion device gives a short-circuit current density (J_{sc}) of 3.46 mA/cm^2 and a fill factor (FF) of 41%. The best device based on **BDT-T-DPP**, in which the alkoxyl is replaced by alkylthienyl, affords an enhanced J_{sc} of 4.66 mA/cm^2 and an improved FF of 47%. For **BDT-T-2T-DPP**, in which another two alkylthienyl groups are further incorporated in the molecular backbone, the J_{sc} is slightly decreased to 4.6 mA/cm^2 and the FF is decreased to 43% compared to the best **BDT-T-DPP** based device. Otherwise, compared to **BDT-O−DPP**, **BDT-T-2T-DPP** also exhibits a higher J_{sc} (3.46 mA/cm^2 vs. 4.6 mA/cm^2) and a higher FF (41% vs. 43%). Except for the J_{sc} and FF, the open-circuit voltage (V_{oc}) is decreased from 0.95 V for **BDT-O-DPP** slightly to 0.92 V for **BDT-T-DPP** and further obviously to 0.83 V for **BDT-T-2T-DPP**. Considering the same device configuration, the variations of V_{oc} are likely associated with the different D/A ratio and largely different phase separated nanostructures between the active layers. As such, due to the different J_{sc}, V_{oc}, and FF, NF-SMSC devices based on **BDT-O-DPP**, **BDT-T-DPP**, and **BDT-T-2T-DPP** exhibited a PCE of 1.34, 2.01, and 1.62%, respectively. Obviously, the evolution tendency of both the J_{sc} and FF, and in turn, the efficiency is different with the conformation-twist trend and the $\pi\pi$-stacking strength trend, and the aggregation ability trend. Noted that the change tendency of the PCE from 1.34 to 2.01%, and 1.62% is in line with the PCE obtained by using PC71BM as acceptor material, going from 1.40% (**BDT-O-DPP**) to 3.88% (**BDT-T-DPP**) and 3.46% (**BDT-T-2T-DPP**) (see Table S3 in the Supporting Information).

Table 3. Photovoltaic Parameters of the Champion Devices with BDT-O-DPP, BDT-T-DPP, and BDT-T-2T-DPP, Respectively, as Donor and Bis-PDI-T-EG as Acceptor

	D/A	DIO (%)	J_{sc} (mA/cm^2)	V_{oc} (V)	FF	PCE (avg%)
BDT-O-DPP	1:1	1.0	3.46	0.95	0.41	1.34 (1.30)
BDT-T-DPP	1.2:1	1.0	4.66	0.92	0.47	2.01 (1.91)
BDT-T-2T-DPP	1:1	1.0	4.60	0.83	0.43	1.62 (1.58)

The external quantum efficiency (EQE) curves of the best NF-SMSC devices are displayed in Figure 7b. The maximum EQE value is of 21, 28, and 28%, respectively, for **BDT-O-DPP**, **BDT-T-DPP**, and **BDT-T-2T-DPP** based NF-SMSC device. This increasing tendency is consistent with the enhanced tendency of the J_{sc} obtained from the $J-V$ curves.

Variations of the J_{sc} and FF are related to the carrier mobility differences. Both the hole and electron mobilities were estimated with space-charge-limited-current (SCLC) method (see Figures S5−S7 in the Supporting Information) and the results are summarized in Table S4 in the Supporting Information. The best **BDT-T-DPP**/bis-PDI-T-EG blend gives a hole/electron mobility of 0.022/0.016 cm^2/(V s), whereas **BDT-O-DPP**/bis-PDI-T-EG blend shows a hole/electron mobility of 0.0011/0.0057 cm^2/(V s) and **BDT-T-2T-DPP**/bis-PDI-T-EG blend yields a hole/electron mobility of 0.0016/0.11 cm^2/(V s). Obviously, in the latter two systems the photocurrent is limited by the lower hole mobility, being on the order of 10^{-3} cm^2/(V s), while the **BDT-T-DPP**/bis-PDI-T-EG system has a balanced carrier mobility, both on the order 10^{-2} cm^2/(V s). The higher carrier mobility and balanced hole and electron mobility of **BDT-T-DPP**/bis-PDI-T-EG system contribute to a higher J_{sc} and a higher FF, and in turn a higher efficiency.

To get deep insights into the structural differences that affect the device performance, phase separated nanostructures were probed using tapping mode atomic force microscopy (AFM) and transmission electron microscopy (TEM) techniques. Figure 8a—c shows the AFM phase images of the active layers of the best devices. The domain size for the three blend films decreases as the following sequence: **BDT-O-DPP**/bis-PDI-T-EG (50—80 nm) > **BDT-T-DPP**/bis-PDI-T-EG (30—50 nm) > **BDT-T-2T-DPP**/bis-PDI-T-EG (10—30 nm), which is well-consistent with the donor aggregation ability, as discussed in the DSC and XRD data. Figure 8d—f shows the TEM images of the blend films of the best devices. Consistent with the AFM phase images, the three blend films display several tens of nanometer sized domains, with the domain size following the same sequence as that obtained from the AFM. The **BDT-T-DPP**/bis-PDI-T-EG film forms a moderate phase domain size of 30−50 nm, with respect to the **BDT-O-DPP**/bis-PDI-T-EG and the **BDT-T-2T-DPP**/bis-PDI-T-EG film, which is beneficial to the balance of exciton dissociation and charge transportation, well-consistent with its balanced hole/electron mobilities and in turn, the highest J_{sc}, FF, and PCE. Again, the smaller phase size for **BDT-T-2T-DPP**/bis-PDI-T-EG film, with respect to that for the **BDT-O-DPP**/bis-PDI-T-EG film, yields higher interface volume density for charge dissociation,

dx.doi.org/10.1021/am406050j | ACS Appl. Mater. Interfaces 2014, 6, 3853−3862

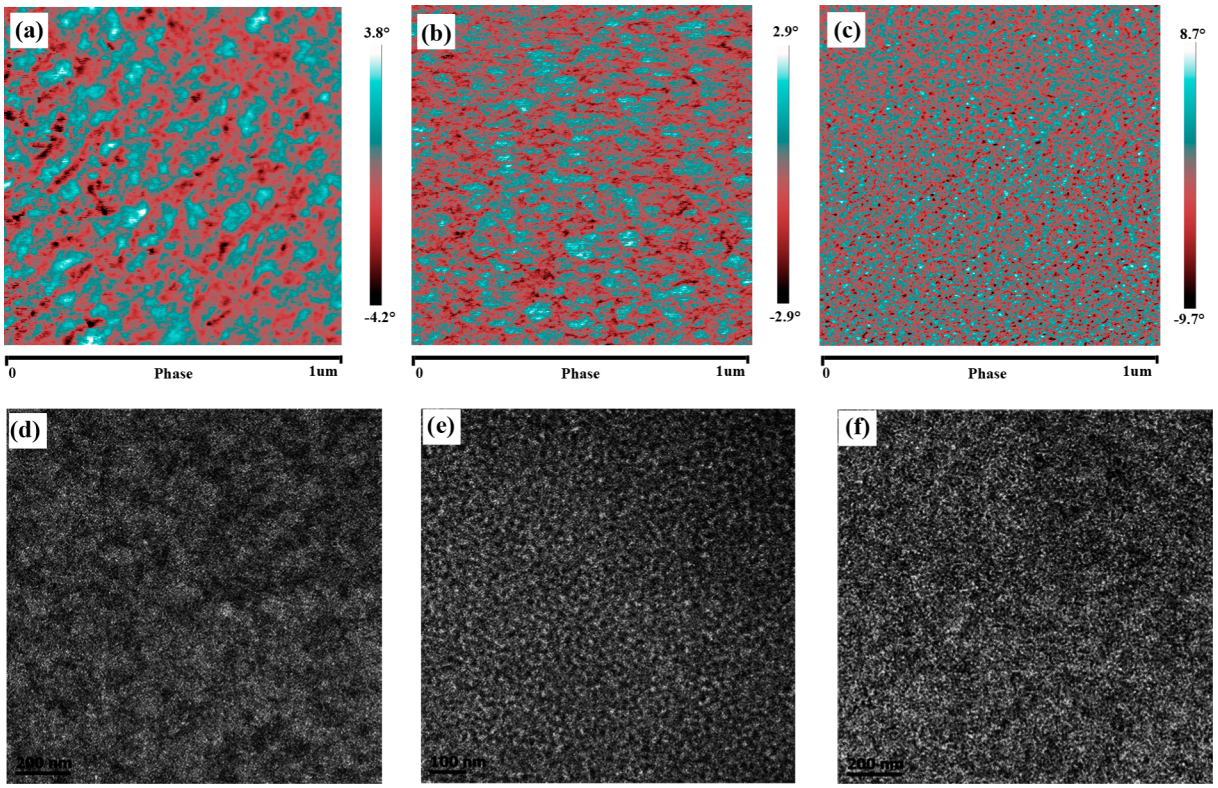

Figure 8. (a–c) AFM phase images and (d–f) TEM images of **BDT-O–DPP**/bis-PDI-T-EG, **BDT-T-DPP**/bis-PDI-T-EG, and **BDT-T-2T-DPP**/bis-PDI-T-EG blend films of the best devices.

accounting for relative higher J_{sc} and PCE from **BDT-T-2T-DPP** than **BDT-O-DPP**. Those results indicate that by anchoring the alkylthienyl at different positions of donor backbones, the domain sizes and the phase separation features of the active layers are adjusted, and then the hole/electron mobilities, J_{sc}, FF, and PCE are adjusted.

Herein, it's worth noting that by adding 1% DIO as co-solvent, the PCE is improved by two order of magnitudes (~0.01% vs. ~1–2%) (see Figure S8a and Table S2 in the Supporting Information). The enhanced efficiency is mainly contributed from the significant increase of J_{sc} and FF. Consistently, the hole and electron mobilities are improved by at least one magnitude after adding 1% DIO as the co-solvent (see Table S3 in the Supporting Information). The increasing hole mobility is contributed from the improved order of the crystallites. As shown in grazing incidence X-ray diffraction (GIXRD, see Figure S9 in the Supporting Information), the neat donor film exhibits an obvious (100) diffraction at q_z = 0.63, 0.62, and 0.56 Å^{-1}, respectively, for **BDT-O-DPP**, **BDT-T-DPP**, and **BDT-T-2T-DPP**. After blended with bis-PDI-T-EG, the (100) diffraction intensity is obviously weakened, demonstrating the interruption of the crystallite order. When 1% DIO is used as co-solvent, the (100) diffraction becomes significantly enhanced for all three blended films, which reveals the remarkable effects of DIO on the ordering of the crystallites, yielding a hopping increase of the hole mobility.

The hopping increase of the device performance is also associated with the dramatic decrease of the phase domain size and the improved compatibility between the donor and acceptor after using 1% DIO as the co-solvent. Figure S11 in the Supporting Information shows the AFM height images of the blended films spin-coated with chloroform and chloroform-DIO, respectively, for comparison. Before adding DIO, the blend film exhibits a value of surface roughness (R_q) of 0.749, 0.648, and 0.377 nm for **BDT-O-DPP**/bis-PDI-T-EG, **BDT-T-DPP**/bis-PDI-T-EG, and **BDT-T-2T-DPP**/bis-PDI-T-EG, respectively (see Figure S11a–c in the Supporting Information). After adding 1% DIO as co-solvent, the R_q value is decreased to 0.291, 0.314, and 0.424 nm for the three blend films (see Figure S11d–f in the Supporting Information), indicating the better compatibility between the donor/acceptor nanostructures. Figure S12 in the Supporting Information shows the AFM phase images and TEM images of the active layers prepared with chloroform as the film-forming solvent. Large phases (> 200 nm) are observed from the three blend films. The phase domain size is remarkably larger than the exciton diffusion length, typically 10 nm,[61] inhibiting the effective exciton diffusion and exciton separation, leading to inferior J_{sc} and FF (see Table S2 in the Supporting Information). Upon adding DIO as co-solvent, the phase domain size is decreased to <80 nm (Figure 8), which is more close to the exciton diffusion length, corresponding to enhanced J_{sc} and FF.

The decreased phase domain size is related to the higher boiling point of DIO than chloroform (332.5 °C vs. 61.3 °C, at 760 mm Hg) and the higher solubility of bis-PDI-T-EG (above 0.2 mg/mL) than those donor materials (lower than 0.05 mg/mL) in DIO. After the main solvent of chloroform is dried during the spin-coating process, more acceptor dissolves in DIO, forming the acceptor-DIO liquid phase, because of the much higher boiling-point of DIO than chloroform. As the poor solubility of the donor in the DIO, the donor molecules is forced to form precipitates after the evaporation of chloroform, consisting of a distribution of amorphous and crystalline regions. During processing of the blending films, the slow evaporation speed of DIO compared to cholorform offers

dx.doi.org/10.1021/am406050j | ACS Appl. Mater. Interfaces 2014, 6, 3853–3862

sufficient time for the acceptor-DIO liquid phase penetrating into the donor phase to form more homogeneous blends to form decreased phase domain size.[35,44]

Accordingly, by adding DIO as co-solvent, the molecular packing order promotes, the miscibility of donor/acceptor improves, the phase domain size decreases, the hole/electron mobilities enhances, and in turn, the PCE hops by two order of magnitude.

4. CONCLUSIONS

Three DPP-based molecules of **BDT-O-DPP**, **BDT-T-DPP**, and **BDT-T-2T-DPP** were synthesized and non-fullerene all-small-molecule solar cells (NF-SMSCs) were fabricated with the three DPP-based molecules, respectively, as the donor material and a PDI-based molecule of bis-PDI-T-EG as the non-fullerene acceptor material. Molecular modeling, UV−vis absorption, DSC and XRD tests indicate that the crystallization and aggregation ability of the three molecules obey the sequence of **BDT-O−DPP** > **BDT-T-DPP** > **BDT-T-2T-DPP**, which is adjusted by incorporating the alkylthienyl unit into the different positions of the backbone. Because of the strong dipolar interactions and better planarity, **BDT-O-DPP** exhibits the strongest aggregation and highest crystallinity. After replacing the alkoxyl by alkylthienyl, the resulting **BDT-T-DPP** shows weaker aggregation ability. Moreover, after the alkylthienyl is further introduced in between the BDT and DPP units, the resulting **BDT-T-2T-DPP** shows even poor planarity and aggregation ability. When blended with the perylene diimide dimer of bis-PDI-T-EG, the moderate aggregation ability of **BDT-T-DPP** yields a moderate phase size of 30−50 nm, whereas the strong aggregation ability of **BDT-O-DPP** gives a bigger size of 50−80 nm and the weak aggregation ability of **BDT-T-2T-DPP** produces a smaller size of 10−30 nm. The best **BDT-T-DPP** based device exhibits a power conversion efficiency (PCE) of 2.01%, whereas the best **BDT-O-DPP** and **BDT-T-2T-DPP** based device gives a PCE of 1.34 and 1.62%, respectively.

5. EXPERIMENTAL SECTION

Materials. All of the starting materials and solvents were purchased from Sigma Aldrich or Alfa Aesar and were used without further purification, unless otherwise stated. Distannyl monomers of BDT (**4a** or **4b**) were purchased from Solarmer. 3-(5-Bromothiophen-2-yl)-2,5-bis(2-ethylhexyl)-6-(thiophen-2-yl)pyrrolo[3,4-c] pyrrole-1,4-(2H,5H)-dione (**6**) was synthesized according to the literature method.[62]

Synthesis of ***4***. Distannyl monomer (**2**, 1 equiv) and 2-bromo-3-hexylthiophene (**3**, 2.5 equiv), were dissolved in dry toluene and degassed with N_2 for 10 min. $Pd(PPh_3)_4$ was added and the solution was degassed with N_2 for another 10 min. The mixture was stirred at 120 °C overnight under the N_2 atmosphere. After being cooled to room temperature, toluene was then evaporated using a rotary evaporator. The residue was purified by column chromatography on silica gel (petrol ether/dichloromethane = 3:1) to give **4** with yield of 78%. ^{1}H NMR (400 MHz, $CDCl_3$, δ, ppm): 7.68 (s, 2H), 7.34 (d, J = 3.2 Hz, 2H), 7.23 (d, J = 4.8 Hz, 2H), 6.95 (d, J = 5.2 Hz, 2H), 6.89 (d, J = 3.2 Hz, 2H), 2.80−2.87 (m, 8H), 1.60−1.69 (m, 6H), 1.27−1.46 (m, 28H), 0.86−0.96 (m, 18H). MS (MALDI-TOF): calcd for $C_{54}H_{70}S_6$, 910.38; found, m/z = 911.50 $[M + H]^+$.

Synthesis of ***5***. **4** (1 equiv) was dissolved in dry THF and cooled to −78 °C and degassed with N_2 for 10 min. n-BuLi dissolved in n-hexane (2.2 M, 2.5 equiv) was then added dropwise. The mixture was raised to room temperature and stirred under N_2 protection for 30 min. Then Me_3SnCl (3 equiv) was added in one portion. The mixture was further stirred under room temperature for 1 h and poured into water for extraction with diethyl ether. The combined organic layers were washed with brine and dried over $MgSO_4$. The solvent was evaporated to obtain yellow oil, which was used for the next reaction without further purification.

Synthesis of **BDT-T-DPP** has been reported in our previous work.[55] **BDT-O-DPP** and **BDT-T-2T-DPP** was synthesized as follow: distannyl monomer (**1**, **2**, or **5**, 1 equiv), **6** (2.5 equiv), and tri(*o*-tolyl)phosphine (16 mol %) were dissolved in dry toluene and degassed with N_2 for 10 min. Tris(dibenzylideneacetone)dipalladium (3 mol %) was added and the solution was degassed with N_2 for another 10 min. The mixture was stirred at 120 °C overnight under the N_2 atmosphere. After cooling down to room temperature, toluene was then evaporated using a rotary evaporator. The residue was purified by column chromatography on silica gel to obtain black solid.

Data for **BDT-O-DPP**. ^{1}H NMR (400 MHz, $CDCl_3$, δ, ppm): 8.98 (d, J = 4.0 Hz, 2H), 8.92 (s, 2H), 7.64 (d, J = 4.4 Hz, 4H), 7.46 (d, J = 3.2 Hz, 2H), 7.28 (t, J_1 = 4.8 Hz, J_2 = 4.8 Hz, 2H), 4.23 (d, J = 4.4 Hz, 4H), 4.07 (m, 8H), 1.84−1.97 (m, 2H), 1.69−1.75 (m, 4H), 1.24−1.58 (m, 48H), 0.95−1.06 (m, 24H). ^{13}C NMR (100 MHz, $CDCl_3$, δ, ppm): 161.65, 144.46, 142.23, 140.23, 139.48, 136.77, 135.70, 135.42, 132.81, 130.58, 129.86, 129.49, 128.46, 126.25, 117.62, 108.52, 108.16, 45.96, 40.69, 39.31, 39.13, 30.46, 30.29, 30.25, 30.22, 39.23, 28.45, 28.37, 23.85, 23.70, 23.56, 23.18, 23.11, 14.24, 14.10, 14.05, 14.36, 10.58. Elemental anal. Calcd for $C_{112}H_{130}N_4O_{14}S_2$: C, 69.22; H, 7.70; N, 3.75. Found: C, 69.30; H, 7.62; N, 3.70. MS (MALDI-TOF): calcd for $C_{112}H_{130}N_4O_{14}S_2$, 1490.71; found, m/z = 1491.35 $[M + H]^+$.

Data for **BDT-T-2T-DPP**. ^{1}H NMR (400 MHz, $CDCl_3$, δ, ppm): 8.92 (d, J = 4.0 Hz, 2H), 8.89 (d, J = 3.2 Hz, 2H), 7.70 (s, 2H), 7.63 (d, J = 8.0 Hz, 2H), 7.35 (d, J = 3.6 Hz, 2H), 7.30 (d, J = 4.0 Hz, 2H), 7.28 (d, J = 5.2 Hz, 2H), 7.17 (s, 2H), 6.93 (d, J = 3.2 Hz, 2H), 4.04 (m, 8H), 2.88 (m, 8H), 1.88 (m, 4H), 1.69 (m, 6H), 1.25−1.45 (m, 56H), 0.84−0.98 (m, 42H). ^{13}C-NMR (100 MHz, $CDCl_3$, δ, ppm): 161.77, 161.55, 146.05, 142.36, 139.84, 139.08, 139.00, 136.98, 138.81, 136.63, 135.16, 134.95, 132.08, 130.37, 129.96, 128.43, 128.36, 128.18, 127.88, 125.52, 124.74, 123.46, 121.82, 108.23, 45.98, 41.54, 39.34, 39.14, 34.36, 32.61, 31.65, 30.49, 30.29, 29.78, 29.32, 28.98, 28.71, 28.42, 25.80, 23.76, 23.63, 23.16, 23.08, 22.65, 14.19, 14.12. Elemental anal. Calcd for $C_{112}H_{130}N_4O_{14}S_2$: C, 69.96; H, 7.52; N, 2.86. Found: C, 69.89; H, 7.60; N, 2.81. MS (MALDI-TOF): calcd for $C_{112}H_{130}N_4O_{14}S_2$, 1954.86; found, m/z = 1955.80 $[M + H]^+$.

■ ASSOCIATED CONTENT

Ⓢ Supporting Information

DFT calculations, measurement details, device preparation and SCLC tests, TGA curves, CV curves, XRD and GIXRD patterns, AFM height images, electrochemical data, photovoltaic data, and NMR spectra. This material is available free of charge via the Internet at http://pubs.acs.org.

■ AUTHOR INFORMATION

Corresponding Authors

*E-mail: clzhan@iccas.ac.cn.

*E-mail: jnyao@iccas.ac.cn.

Author Contributions

The manuscript was written through contributions of all authors. All authors have given approval to the final version of the manuscript.

Notes

The authors declare no competing financial interest.

■ ACKNOWLEDGMENTS

This work is financially supported by NSFC (21327805, 91227112, and 21221002), Chinese Academy of Sciences and Projects 973 (2011CB808400). A portion of this work is based on the data obtained at 1W1A, BSRF. The authors gratefully

acknowledge the assistance of the scientists at Diffuse X-ray Scattering Station, BSRF, during the experiments.

REFERENCES

(1) Chen, J. W.; Cao, Y. Development of Novel Conjugated Donor Polymers for High-Efficiency Bulk-Heterojunction Photovoltaic Devices. *Acc. Chem. Res.* **2009**, *42*, 1709−1718.

(2) Cheng, Y. J.; Yang, S. H.; Hsu, C. S. Synthesis of Conjugated Polymers for Organic Solar Cell Applications. *Chem. Rev.* **2009**, *109*, 5868−5923.

(3) Yip, H.-L.; Jen, A. K. Y. Recent Advances in Solution-Processed Interfacial Materials for Efficient and Stable Polymer Solar Cells. *Energy Environ. Sci.* **2012**, *5*, 5994−6011.

(4) Zhou, H.; Yang, L.; You, W. Rational Design of High Performance Conjugated Polymers for Organic Solar Cells. *Macromolecules* **2012**, *45*, 607−632.

(5) Zhou, J.; Wan, X.; Liu, Y.; Zuo, Y.; Li, Z.; He, G.; Long, G.; Ni, W.; Li, C.; Su, X.; Chen, Y. Small Molecules Based on Benzo[1,2-b:4,5-b′]dithiophene Unit for High-Performance Solution-Processed Organic Solar Cells. *J. Am. Chem. Soc.* **2012**, *134*, 16345−16351.

(6) Zhou, J.; Zuo, Y.; Wan, X.; Long, G.; Zhang, Q.; Ni, W.; Liu, Y.; Li, Z.; He, G.; Li, C.; Kan, B.; Li, M.; Chen, Y. Solution-Processed and High-Performance Organic Solar Cells Using Small Molecules with a Benzodithiophene Unit. *J. Am. Chem. Soc.* **2013**, *135*, 8484−8487.

(7) Lin, Y.; Li, Y.; Zhan, X. Small Molecule Semiconductors for High-Efficiency Organic Photovoltaics. *Chem. Soc. Rev.* **2012**, *41*, 4245−4272.

(8) Demeter, D.; Jeux, V.; Leriche, P.; Blanchard, P.; Olivier, Y.; Cornil, J.; Po, R.; Roncali, J. Tuning of the Photovoltaic Parameters of Molecular Donors by Covalent Bridging. *Adv. Funct. Mater.* **2013**, *23*, 4854−4861.

(9) Dutta, P.; Yang, W.; Eom, S. H.; Lee, W. H.; Kang, I. N.; Lee, S. H. Development of Naphtho[1,2-*b*:5,6-*b*′]dithiophene Based Novel Small Molecules for Efficient Bulk-Heterojunction Organic Solar Cells. *Chem. Commun.* **2012**, *48*, 573−575.

(10) Hou, Q.; Chen, Y.; Zhen, H.; Ma, Z.; Hong, W.; Shi, G.; Zhang, F. A Triphenylamine-Based Four-Armed Molecule for Solution-Processed Organic Solar Cells with High Photo-Voltage. *J. Mater. Chem. A* **2013**, *1*, 4937−4940.

(11) Huang, J.; Jia, H.; Li, L.; Lu, Z.; Zhang, W.; He, W.; Jiang, B.; Tang, A.; Tan, Z.; Zhan, C.; Li, Y.; Yao, J. Fine-Tuning Device Performances of Small Molecule Solar Cells via the More Polarized DPP-Attached Donor Units. *Phys. Chem. Chem. Phys.* **2012**, *14*, 14238−14242.

(12) Kang, S. J.; Ahn, S.; Kim, J. B.; Schenck, C.; Hiszpanski, A. M.; Oh, S.; Schiros, T.; Loo, Y. L.; Nuckolls, C. Using Self-Organization to Control Morphology in Molecular Photovoltaics. *J. Am. Chem. Soc.* **2013**, *135*, 2207−2212.

(13) Kim, J.; Ko, H. M.; Cho, N.; Paek, S.; Lee, J. K.; Ko, J. Efficient Small Molecule Organic Semiconductor Containing Bis-dimethylfluorenyl Amino Benzo[*b*]thiophene for High Open Circuit Voltage in High Efficiency Solution Processed Organic Solar Cell. *RSC Adv.* **2012**, *2*, 2692−2695.

(14) Lam, S. L.; Liu, X.; Zhao, F.; Lee, C. L.; Kwan, W. L. Manipulating Open-Circuit Voltage in an Organic Photovoltaic Device via a Phenylalkyl Side Chain. *Chem. Commun.* **2013**, *49*, 4543−4545.

(15) Lee, O. P.; Yiu, A. T.; Beaujuge, P. M.; Woo, C. H.; Holcombe, T. W.; Millstone, J. E.; Douglas, J. D.; Chen, M. S.; Frechet, J. M. Efficient Small Molecule Bulk Heterojunction Solar Cells with High Fill Factors via Pyrene-Directed Molecular Self-Assembly. *Adv. Mater.* **2011**, *23*, 5359−5363.

(16) Li, P.; Tong, H.; Ding, J.; Xie, Z.; Wang, L. Small Molecules Based on 2,7-Carbazole for Efficient Solution-Processed Organic Solar Cells. *J. Mater. Chem. A* **2013**, *1*, 8805−8812.

(17) Li, Z.; Dong, Q.; Li, Y.; Xu, B.; Deng, M.; Pei, J.; Zhang, J.; Chen, F.; Wen, S.; Gao, Y.; Tian, W. Design and Synthesis of Solution Processable Small Molecules Towards High Photovoltaic Performance. *J. Mater. Chem.* **2011**, *21*, 2159−2166.

(18) Liu, J.; Sun, Y.; Moonsin, P.; Kuik, M.; Proctor, C. M.; Lin, J.; Hsu, B. B.; Promarak, V.; Heeger, A. J.; Nguyen, T. Q. Tri-Diketopyrrolopyrrole Molecular Donor Materials for High-Performance Solution-Processed Bulk Heterojunction Solar Cells. *Adv. Mater.* **2013**, *25*, 5898−5903.

(19) Liu, Y.; Yang, Y. M.; Chen, C. C.; Chen, Q.; Dou, L.; Hong, Z.; Li, G.; Yang, Y. Solution-Processed Small Molecules Using Different Electron Linkers for High-Performance Solar Cells. *Adv. Mater.* **2013**, *25*, 4657−4662.

(20) Pan, J. Y.; Zuo, L. J.; Hu, X. L.; Fu, W. F.; Chen, M. R.; Fu, L.; Gu, X.; Shi, H. Q.; Shi, M. M.; Li, H. Y.; Chen, H. Z. Star-Shaped D-A Small Molecules Based on Diketopyrrolopyrrole and Triphenylamine for Efficient Solution-Processed Organic Solar Cells. *ACS Appl. Mater. Interfaces* **2013**, *5*, 972−980.

(21) Ripaud, E.; Rousseau, T.; Leriche, P.; Roncali, J. Unsymmetrical Triphenylamine-Oligothiophene Hybrid Conjugated Systems as Donor Materials for High-Voltage Solution-Processed Organic Solar Cells. *Adv. Energy Mater.* **2011**, *1*, 540−545.

(22) Schulz, G. L.; Mastalerz, M.; Ma, C.-Q.; Wienk, M.; Janssen, R.; Bäuerle, P. Synthesis and Photovoltaic Performance of Pyrazinoquinoxaline Containing Conjugated Thiophene-Based Dendrimers and Polymers. *Macromolecules* **2013**, *46*, 2141−2151.

(23) Shen, S.; Jiang, P.; He, C.; Zhang, J.; Shen, P.; Zhang, Y.; Yi, Y.; Zhang, Z.; Li, Z.; Li, Y. Solution-Processable Organic Molecule Photovoltaic Materials with Bithienyl-benzodithiophene Central Unit and Indenedione End Groups. *Chem. Mater.* **2013**, *25*, 2274−2281.

(24) Shin, W.; Yasuda, T.; Watanabe, G.; Yang, Y. S.; Adachi, C. Self-Organizing Mesomorphic Diketopyrrolopyrrole Derivatives for Efficient Solution-Processed Organic Solar Cells. *Chem. Mater.* **2013**, *25*, 2549−2556.

(25) Tamayo, A. B.; Walker, B.; Nguyen, T. Q. A Low Band Gap, Solution Processable Oligothiophene with a Diketopyrrolopyrrole Core for Use in Organic Solar Cells. *J. Phys. Chem. C* **2008**, *112*, 11545−11551.

(26) Wang, H.-Y.; Gao, J.; Gu, L.-J.; Wan, J.-H.; Wei, W.; Liu, F. Structural Modification of Thieno[3,4-c]pyrrole-4,6-dione: Structure−Property Relationships and Application in Solution-Processed Small-Molecule Organic Solar Cells. *J. Mater. Chem. A* **2013**, *1*, 5875−5885.

(27) Ye, D.; Li, X.; Yan, L.; Zhang, W.; Hu, Z.; Liang, Y.; Fang, J.; Wong, W.-Y.; Wang, X. Dithienosilole-Bridged Small Molecules with Different Alkyl Group Substituents for Organic Solar Cells Exhibiting High Open-Circuit Voltage. *J. Mater. Chem. A* **2013**, *1*, 7622−7629.

(28) Zeng, S.; Yin, L.; Ji, C.; Jiang, X.; Li, K.; Li, Y.; Wang, Y. D−π−A−π−D Type Benzothiadiazole−Triphenylamine Based Small Molecules Containing Cyano on the π-Bridge for Solution-Processed Organic Solar Cells with High Open-Circuit Voltage. *Chem. Commun.* **2012**, *48*, 10627−10629.

(29) Kyaw, A. K. K.; Wang, D. H.; Gupta, V.; Leong, W. L.; Ke, L.; Bazan, G. C.; Heeger, A. J. Intensity Dependence of Current−Voltage Characteristics and Recombination in High-Efficiency Solution-Processed Small-Molecule Solar Cells. *ACS Nano* **2013**, *7*, 4569−4577.

(30) He, Y.; Chen, H.; Hou, J.; Li, Y. Indene−C_{60} Bisadduct: A New Acceptor for High-Performance Polymer Solar Cells. *J. Am. Chem. Soc.* **2010**, *132*, 1377−1382.

(31) Anctil, A.; Babbitt, C. W.; Raffaelle, R. P.; Landi, B. J. Material and Energy Intensity of Fullerene Production. *Environ. Sci. Technol.* **2011**, *45*, 2353−2359.

(32) Sonar, P.; Fong Lim, J. P.; Chan, K. L. Organic Non-Fullerene Acceptors for Organic Photovoltaics. *Energy Environ. Sci.* **2011**, *4*, 1558−1574.

(33) Zhan, X.; Facchetti, A.; Barlow, S.; Marks, T. J.; Ratner, M. A.; Wasielewski, M. R.; Marder, S. R. Rylene and Related Diimides for Organic Electronics. *Adv. Mater.* **2011**, *23*, 268−284.

(34) Moore, J. R.; Albert-Seifried, S.; Rao, A.; Massip, S.; Watts, B.; Morgan, D. J.; Friend, R. H.; McNeill, C. R.; Sirringhaus, H. Polymer Blend Solar Cells Based on a High-Mobility Naphthalenediimide-Based Polymer Acceptor: Device Physics, Photophysics and Morphology. *Adv. Energy Mater.* **2011**, *1*, 230−240.

(35) Zhou, E.; Cong, J.; Wei, Q.; Tajima, K.; Yang, C.; Hashimoto, K. All-Polymer Solar Cells from Perylene Diimide Based Copolymers: Material Design and Phase Separation Control. *Angew. Chem., Int. Ed.* **2011**, *50*, 2799−2803.
(36) Zhou, Y.; Yan, Q.; Zheng, Y.; Wang, J.; Zhao, D.; Pei, J. New Polymer Acceptors for Organic Solar Cells: the Effect of Regio-Regularity and Device Configuration. *J. Mater. Chem. A* **2013**, *1*, 6609−6613.
(37) Ahmed, E.; Ren, G.; Kim, F. S.; Hollenbeck, E. C.; Jenekhe, S. A. Design of New Electron Acceptor Materials for Organic Photovoltaics: Synthesis, Electron Transport, Photophysics, and Photovoltaic Properties of Oligothiophene-Functionalized Naphthalene Diimides. *Chem. Mater.* **2011**, *23*, 4563−4577.
(38) Bloking, J. T.; Han, X.; Higgs, A. T.; Kastrop, J. P.; Pandey, L.; Norton, J. E.; Risko, C.; Chen, C. E.; Brédas, J.-L.; McGehee, M. D.; Sellinger, A. Solution-Processed Organic Solar Cells with Power Conversion Efficiencies of 2.5% using Benzothiadiazole/Imide-Based Acceptors. *Chem. Mater.* **2011**, *23*, 5484−5490.
(39) Brunetti, F. G.; Gong, X.; Tong, M.; Heeger, A. J.; Wudl, F. Strain and Hückel Aromaticity: Driving Forces for a Promising New Generation of Electron Acceptors in Organic Electronics. *Angew. Chem., Int. Ed.* **2010**, *49*, 532−536.
(40) Howard, I. A.; Laquai, F.; Keivanidis, P. E.; Friend, R. H.; Greenham, N. C. Perylene Tetracarboxydiimide as an Electron Acceptor in Organic Solar Cells: A Study of Charge Generation and Recombination. *J. Phys. Chem. C* **2009**, *113*, 21225−21232.
(41) Jiang, B.; Zhang, X.; Zhan, C.; Lu, Z.; Huang, J.; Ding, X.; He, S.; Yao, J. Benzodithiophene Bridged Dimeric Perylene Diimide Amphiphiles as Efficient Solution-Processed Non-Fullerene Small Molecules. *Polym. Chem.* **2013**, *4*, 4631−4638.
(42) Kamm, V.; Battagliarin, G.; Howard, I. A.; Pisula, W.; Mavrinskiy, A.; Li, C.; Mullen, K.; Laquai, F. Polythiophene:Perylene Diimide Solar Cells − the Impact of Alkyl-Substitution on the Photovoltaic Performance. *Adv. Energy Mater.* **2011**, *1*, 297−302.
(43) Li, H.; Kim, F. S.; Ren, G.; Hollenbeck, E. C.; Subramaniyan, S.; Jenekhe, S. A. Tetraazabenzodifluoranthene Diimides: Building Blocks for Solution-Processable n-Type Organic Semiconductors. *Angew. Chem., Int. Ed.* **2013**, *52*, 5513−5517.
(44) Lu, Z.; Zhang, X.; Zhan, C.; Jiang, B.; Chen, L.; Yao, J. Impact of Molecular Solvophobicity *vs.* Solvophilicity on Device Performances of Dimeric Perylene Diimide Based Solution-Processed Non-Fullerene Organic Solar Cells. *Phys. Chem. Chem. Phys.* **2013**, *15*, 11375−11385.
(45) Schwenn, P. E.; Gui, K.; Nardes, A. M.; Krueger, K. B.; Lee, K. H.; Mutkins, K.; Rubinstein-Dunlop, H.; Shaw, P. E.; Kopidakis, N.; Burn, P. L.; Meredith, P. A Small Molecule Non-fullerene Electron Acceptor for Organic Solar Cells. *Adv. Energy Mater.* **2011**, *1*, 73−81.
(46) Zhou, T.; Jia, T.; Kang, B.; Li, F.; Fahlman, M.; Wang, Y. Nitrile-Substituted QA Derivatives: New Acceptor Materials for Solution-Processable Organic Bulk Heterojunction Solar Cells. *Adv. Energy Mater.* **2011**, *1*, 431−439.
(47) Zhou, Y.; Dai, Y.; Zheng, Y.; Wang, X.; Wang, J.; Pei, J. Non-Fullerene Acceptors Containing Fluoranthene-Fused Imides for Solution-Processed Inverted Organic Solar Cells. *Chem. Commun.* **2013**, *49*, 5802−5804.
(48) Kamm, V.; Battagliarin, G.; Howard, I. A.; Pisula, W.; Mavrinskiy, A.; Li, C.; Müllen, K.; Laquai, F. Polythiophene: Perylene Diimide Solar Cells-the Impact of Alkyl-Substitution on the Photovoltaic Performance. *Adv. Energy Mater.* **2011**, *1*, 297−302.
(49) Rajaram, S.; Shivanna, R.; Kandappa, S. K.; Narayan, K. S. Nonplanar Perylene Diimides as Potential Alternatives to Fullerenes in Organic Solar Cells. *J. Phys. Chem. Lett.* **2012**, *3*, 2405−2408.
(50) Zhang, X.; Lu, Z.; Ye, L.; Zhan, C.; Hou, J.; Zhang, S.; Jiang, B.; Zhao, Y.; Huang, J.; Zhang, S.; Liu, Y.; Shi, Q.; Liu, Y.; Yao, J. A Potential Perylene Diimide Dimer-Based Acceptor Material for Highly Efficient Solution-Processed Non-Fullerene Organic Solar Cells with 4.03% Efficiency. *Adv. Mater.* **2013**, *25*, 5791−5797.
(51) Mikroyannidis, J. A.; Suresh, P.; Sharma, G. D. Synthesis of A Perylene Bisimide with Acetonaphthopyrazine Dicarbonitrile Terminal Moieties for Photovoltaic Applications. *Synth. Met.* **2010**, *160*, 932−938.
(52) Sharenko, A.; Proctor, C. M.; van der Poll, T. S.; Henson, Z. B.; Nguyen, T. Q.; Bazan, G. C. A High-Performing Solution-Processed Small Molecule: Perylene Diimide Bulk Heterojunction Solar Cell. *Adv. Mater.* **2013**, *25*, 4403−4406.
(53) Beaujuge, P. M.; Frechet, J. M. Molecular Design and Ordering Effects in π-Functional Materials for Transistor and Solar Cell Applications. *J. Am. Chem. Soc.* **2011**, *133*, 20009−20029.
(54) Gunes, S.; Neugebauer, H.; Sariciftci, N. S. Conjugated Polymer-Based Organic Solar Cells. *Chem. Rev.* **2007**, *107*, 1324−1338.
(55) Huang, J.; Zhan, C.; Zhang, X.; Zhao, Y.; Lu, Z.; Jia, H.; Jiang, B.; Ye, J.; Zhang, S.; Tang, A.; Liu, Y.; Pei, Q.; Yao, J. Solution-Processed DPP-Based Small Molecule that Gives High Photovoltaic Efficiency with Judicious Device Optimization. *ACS Appl. Mater. Interfaces* **2013**, *5*, 2033−2039.
(56) Huang, J.; Zhao, Y.; Ding, X.; Jia, H.; Jiang, B.; Zhang, Z.; Zhan, C.; He, S.; Pei, Q.; Li, Y.; Liu, Y.; Yao, J. Synthesis and Charge-Transporting Properties of Electron-Deficient CN_2−Fluorene Based D−A Copolymers. *Polym. Chem.* **2012**, *3*, 2170−2177.
(57) Huo, L.; Zhang, S.; Guo, X.; Xu, F.; Li, Y.; Hou, J. Replacing Alkoxy Groups with Alkylthienyl Groups: A Feasible Approach to Improve the Properties of Photovoltaic Polymers. *Angew. Chem., Int. Ed.* **2011**, *50*, 9697−9702.
(58) Takacs, C. J.; Sun, Y.; Welch, G. C.; Perez, L. A.; Liu, X.; Wen, W.; Bazan, G. C.; Heeger, A. J. Solar Cell Efficiency, Self-Assembly, and Dipole−Dipole Interactions of Isomorphic Narrow-Band-Gap Molecules. *J. Am. Chem. Soc.* **2012**, *134*, 16597−16606.
(59) Huang, J.; Wang, X.; Zhan, C.; Zhao, Y.; Sun, Y.; Pei, Q.; Liu, Y.; Yao, J. Wide Band Gap Copolymers Based on Phthalimide: Synthesis, Characterization, and Photovoltaic Properties with 3.70% Efficiency. *Polym. Chem.* **2013**, *4*, 2174−2180.
(60) Langford, J. I.; Wilson, A. J. C. Scherrer after Sixty Years: A Survey and Some New Results in the Determination of Crystallite Size. *J. Appl. Crystallogr.* **1978**, *11*, 102−113.
(61) Nunzi, J. M. Organic Photovoltaic Materials and Devices. *C. R. Phys.* **2002**, *3*, 523−542.
(62) Loser, S.; Bruns, C. J.; Miyauchi, H.; Ortiz, R. P.; Facchetti, A.; Stupp, S. I.; Marks, T. J. A Naphthodithiophene-Diketopyrrolopyrrole Donor Molecule for Efficient Solution-Processed Solar Cells. *J. Am. Chem. Soc.* **2011**, *133*, 8142−8145.